Path integral Monte Carlo on a sphere

Riccardo Fantoni *

Università di Trieste, Dipartimento di Fisica, strada Costiera 11, 34151 Grignano, Trieste, Italy

(Received 30 March 2026; revised 24 June 2026; accepted 21 August 2026; published 8 September 2026)

We solve numerically exactly a simple toy model to quantum general relativity or more properly to path integral on a curved space. We consider the thermal equilibrium of a quantum many-body problem on the sphere, the surface of constant positive curvature. We use path integral Monte Carlo to measure the kinetic energy, the internal energy, and the static structure of a bosons, fermions, and anyons fluid at low temperatures on the sphere. For bosons we also measure the superfluid fraction and compare its behavior at the critical temperature with the universal jump predicted by Nelson and Kosterlitz in flat space in the thermodynamic limit at the superfluid phase transition. For fermions and anyons it is necessary to use the restricted path integral recipe to overcome the sign problem. Even if this recipe is exact for the noninteracting fluid it reduces to just an approximation for an interacting system. And we make the example of the electron gas at low temperature. Snapshots of the many-body path configuration during the evolution of the computer experiment show that the "speed" of the single-particle path near the poles slows down as a consequence of the "hairy ball theorem" of Poincaré. The influence of curvature on the thermodynamic and structural properties of the many-body fluid is also studied.

DOI: 10.1103/y457-glbg

I. INTRODUCTION

One of the greatest challenges of physics today is the problem of putting together the quantum theory with the theory of general relativity, or from the mathematical side we are looking forward to a bridge between the functional integral underlying the time evolution in a Hilbert space and the Riemannian manifold underlying the support of differential geometry or more generally differential topology. We are still at the beginning of this ambitious project and from this point of view any simple, yet well-defined, physical model at the intersection of these two theories is certainly valuable, especially so if the model can be solved exactly from a mathematical point of view [1,2].

From the laboratory experimental point of view we must stress that in recent years some extraordinary advances have been made in the manufacturing of cold quantum gases trapped on various geometries [3,4]. The advances in the realization of trapped *Bose-Einstein condensates* [5–11] has interests in the construction of quantum interferometry sensors, atomic lasers, or quantum computers. Whereas trapped electron liquids have been realized in nuclear fusion experiments. Only recently we have been able to create a white dwarf artificially in a earthly laboratory [12]. This is one more reason to study the properties of *Jellium* [13–16], an electron liquid where the ionic component is approximated by a uniform neutralizing background stabilizing the plasma. This is just a first brute approximation to the more realistic model of a two component plasma [17,18]; but even so it poses the extremely challenging problem of the determination of the ground state and low temperature properties of a many electron system on a curved spacetime [19,20] with the additional subtleties of overcoming the fermions sign problem [21–23] and ordering problems on properly defined self adjoint operators subject to holonomic constraints as the ones faced in the development of a quantum theory of curved spacetime [1,24–26].

Guided by these motivations some years ago we studied the statistical physics problem of an electron gas at finite, nonzero temperature on the surface of a sphere [19,20], the surface of constant positive curvature and probably the simplest of all Riemannian manifolds. Similar studies on the Haldane sphere had already been tried but at zero temperature [27–29]. And at high temperature, at a special value of the Coulomb coupling constant, in the nonquantum regime, on several different (curved) surfaces: the plane [30–33], the cylinder [34,35], the sphere [36–39], the pseudosphere [40–42], and the Flamm paraboloid [43,44]. Other authors [45] studied the electron gas on a sphere within linear response theory.

Here we want to examine carefully the case of a many-body system on a sphere at finite, nonzero low temperature, i.e., in its quantum regime. The thermal equilibrium properties of the many-body system will be captured by a path integral description of its density matrix on the sphere.

The bodies that form the statistical physics model can be described either as distinguishable or as identical. In their description as identical bodies we can further distinguish between whether they obey to Bose-Einstein statistics or if they obey to Fermi-Dirac statistics according to their wave function transformation property under their permutation. If

*Contact author: riccardo.fantoni@scuola.istruzione.it

additionally they are described as identical and impenetrable bodies they will obey to anyonic statistics according to their wave function imaginary time braiding evolution. The braid group was introduced in 1925 by Emil Artin [46]. All these descriptions bring to different statistical physics and thermodynamic properties when the many-body system is in its low temperature quantum regime, and they merge at high temperature [47].

On the other side, already the simple sphere has some quite delicate features as, for example, the *hairy ball theorem*, according to which her Euler class is the obstruction to her tangent planes, the *tangent bundle*,[1] having always a nonvanishing *fiber*, or hair, for any *section*.[2] The theorem was first proven by Henri Poincaré for the sphere in 1885 [48], and extended to higher even dimensions in 1912 by Luitzen Egbertus Jan Brouwer [49]. The theorem has been expressed colloquially as "you can't comb a hairy ball flat without creating a cowlick." If f is a continuous function that assigns a vector in the three-dimensional space to every point $\boldsymbol{r}$ on a sphere such that $f(\boldsymbol{r})$ is always tangent to the sphere at $\boldsymbol{r}$, then there is at least one *pole*, a point where the field vanishes, i.e., an $\boldsymbol{r}$ such that $f(\boldsymbol{r})=0$. Every zero of a vector field has a (nonzero) *index*,[3] and it can be shown that the sum of all of the indexes at all of the zeros must be two, because the Euler characteristic of the sphere is two. Therefore, there must be at least one zero. This is a consequence of the *Poincaré-Hopf theorem*. The theorem was proven for two dimensions by Henri Poincaré and later generalized to higher dimensions by Heinz Hopf [50]. In particular, we expect that even a single free particle in thermal equilibrium at low temperature on the sphere have a path which will be subject to some peculiar topological features [51].

The question of the influence on the statistical physics properties of a quantum many-body fluid of the curvature of the supporting Riemannian surface is not straightforward. In fact, already for a single free particle the phase space dynamics on a sphere is generally not ergodic since her trajectories, the geodesics, may be confined to invariant tori, but the picture dramatically changes on a pseudosphere, *the* surface of constant negative curvature, as was proven by Artin in 1924 [52], where geodesics diverge [41,53]. This makes the quantum version of this system a paradigmatic model of quantum chaos.

We then here plan to study this preliminary simple toy model of a quantum many-body fluid on a sphere, which nonetheless does not allow for an analytic exact solution, with the instrument of path integral Monte Carlo (PIMC) [23], which is able to extract exact numerical properties of the statistical physics model. It certainly is gratifying to know that at least this simple toy model of statistical general relativity [24–26] can be solved exactly at least numerically.

II. MANY-BODY PATH INTEGRAL ON A RIEMANNIAN MANIFOLD

Throughout the paper we will denote with a bold face letter a point on the d-dimensional Riemannian manifold $\mathcal{M}$. Greek indexes run over the d space dimensions. Roman indexes are used either for a particle label or for an imaginary timeslice label in the path integral discretization. We use Einstein summation convention of tacitly assuming a sum over repeated Greek indexes.

A many-body system is composed of N *distinguishable* particles of mass m and spin s with positions in $R=(\boldsymbol{r}_1,\boldsymbol{r}_2,\ldots,\boldsymbol{r}_N)=(\{\boldsymbol{r}_i\})$ where each position vector $\boldsymbol{r}_i=(r_i^1,r_i^2,\ldots,r_i^d)=(\{r_i^\alpha\})$ in d dimensions. On a Riemannian manifold $\mathcal{M}$ of dimension d and metric tensor $g_{\alpha\beta}(\boldsymbol{r})$, the geodesic distance between two infinitesimally close points R and R' is $d\tilde{s}^2(R,R')=\sum_{i=1}^N ds^2(\boldsymbol{r}_i,\boldsymbol{r}'_i)$ where $ds^2(\boldsymbol{r},\boldsymbol{r}')=g_{\alpha\beta}(\boldsymbol{r})(\boldsymbol{r}-\boldsymbol{r}')^\alpha(\boldsymbol{r}-\boldsymbol{r}')^\beta$. Moreover,

$$\tilde{g}_{\mu\nu}(R)=g_{\alpha_1\beta_1}(\boldsymbol{r}_1)\otimes\ldots\otimes g_{\alpha_N\beta_N}(\boldsymbol{r}_N), \tag{2.1}$$

$$\tilde{g}(R)=\prod_{i=1}^N \det||g_{\alpha_i\beta_i}(\boldsymbol{r}_i)||, \tag{2.2}$$

where $||\tilde{g}_{\mu\nu}||$ is a matrix made of N diagonal blocks $||g_{\alpha_i\beta_i}||$ with $i=1,2,\ldots,N$. The Laplace-Beltrami operator on the manifold of dimension dN is

$$\Delta_R=\tilde{g}^{-1/2}\nabla_\mu(\tilde{g}^{1/2}\tilde{g}^{\mu\nu}\nabla_\nu), \tag{2.3}$$

where $\boldsymbol{\nabla}=\boldsymbol{\nabla}_R$, $\tilde{g}^{\gamma\nu}$ is the inverse of $\tilde{g}_{\gamma\nu}$, i.e., $\tilde{g}_{\mu\gamma}\tilde{g}^{\gamma\nu}=\delta_\mu{}^\nu$ the Kronecker δ.

We will first assume *free*, noninteracting bodies, with an Hamiltonian $\mathcal{H}$ that reduces to the one of the free gas in flat space. For the sake of simplicity,[4] we will choose

$$\mathcal{H}=-\lambda\Delta_R, \tag{2.4}$$

with $\lambda=\hbar^2/2m$.

For *interacting* bodies we will then have more generally

$$\mathcal{H}=-\lambda\Delta_R+V(R), \tag{2.5}$$

where $V(R)$ is the *physical potential* energy of the system, that we here assume only a function of the particles positions and bounded from below.

The density matrix ρ of the system obeys to Bloch equation

$$\frac{\partial\rho(t)}{\partial t}=-\mathcal{H}\rho(t), \tag{2.6}$$

$$\rho(0)=\mathbb{1}, \tag{2.7}$$

where t is the imaginary time with dimension of the reciprocal of energy and $\mathbb{1}$ the identity matrix. The position representation of the density matrix is then obtained from $\rho(R,R';t)=\langle R|\rho(t)|R'\rangle$ with $\langle R|R'\rangle=\delta(R-R')/\sqrt{\tilde{g}(R)}$

[1] A particular *fiber bundle*.

[2] In topology, a cross *section* of a fiber (tangent) bundle space, $B\times F$ is a graph over the *base space* B, in this case the sphere. A choice of a tangent vector to any point of the sphere is a section of the tangent bundle of the sphere.

[3] The index of a bilinear function/al is the dimension of the space on which it is negative definite. In the context of vector fields on a Riemannian manifold the index is equal to $+1$ around a source or a sink, and more generally equal to $(-1)^k$ around a saddle that has k contracting dimensions and $n-k$ expanding dimensions.

[4] This is a delicate point especially for what concerns ordering ambiguities [1]. We here appeal to simplicity.

where δ is a dN-dimensional Dirac δ function. In the small imaginary time τ limit the position representation of the density matrix is

$$\rho(R,R';\tau) \propto \tilde{g}(R)^{-1/4}\sqrt{\mathcal{D}(R,R';\tau)}\,\tilde{g}(R')^{-1/4} \times e^{\lambda\tau\mathcal{R}(R)/6}e^{-\mathcal{S}(R,R';\tau)}, \quad (2.8)$$

where $\mathcal{R}$ is the scalar curvature of the manifold,[5] $\mathcal{S}$ the action, and $\mathcal{D}$ the van Vleck's determinant [55,56]

$$\mathcal{D}_{\mu\nu} = -\nabla_\mu\nabla'_\nu\mathcal{S}(R,R';\tau), \quad (2.9)$$

$$\det||\mathcal{D}_{\mu\nu}|| = \mathcal{D}(R,R';\tau), \quad (2.10)$$

where $\nabla = \nabla_R$ and $\nabla' = \nabla_{R'}$. This determinant is the Jacobian of the transformation from the initial conditions given by fixing the pair of momentum and coordinate to the boundary conditions given by specifying the pair of initial and final coordinates needed in the coordinate representation. The square root of the van Vleck determinant factor takes into account the density of paths among the minimum extremal region for the action (see Chapter 12 of Ref. [56]). For the density matrix (2.8) the volume element of integration is $\sqrt{\tilde{g}(R)}\,dR$. The two factors $\tilde{g}^{-1/4}$ are needed to have for the density matrix a bidensity for which the boundary condition to Bloch equation is simply a Dirac δ function. In the small $\tau\to 0$ limit,[6] $\tilde{g}(R)^{-1/4}\sqrt{D(R,R';\tau)}\,\tilde{g}(R')^{-1/4} \to (1/2\lambda\tau)^N$.

For the *action* $\mathcal{S}$, the *kinetic-action* $\mathcal{K}$, and the *interaction* $\mathcal{U}$ we have[7]

$$\mathcal{S}(R,R';\tau) = \mathcal{K}(R,R';\tau) + \mathcal{U}(R,R';\tau), \quad (2.11)$$

$$\mathcal{K}(R,R';\tau) = \frac{dN}{2}\ln(4\pi\lambda\tau) + \frac{d\tilde{s}^2(R,R')}{4\lambda\tau}. \quad (2.12)$$

In particular, the kinetic-action is responsible for a diffusion of the random walk with a single-particle variance equal to $\sigma^2_{\alpha\beta}(\boldsymbol{r}) = 2\lambda\tau/g_{\alpha\beta}(\boldsymbol{r})$. The interaction is defined as $\mathcal{U} = \mathcal{S} - \mathcal{K}$ and for potential energies bounded from below one can resort to the Trotter formula [57] to reach the *primitive approximation*[8]

$$\mathcal{U}(R,R';\tau) = \tau[V(R) + V(R')]/2. \quad (2.13)$$

For noninteracting bodies $\mathcal{U} = 0$. Note that, even to lowest order in $R - R'$,[9] the path integral in the curved manifold for the noninteracting system will not coincide with the one in flat space since it is not possible with a change of coordinates to simply remove the metric factor from both $d\tilde{s}^2$ and the volume element of integration, if not only locally. In fact, this would require a *noncoordinate basis* [58].

Given then an observable $\mathcal{O}$ we can determine its thermal average at an absolute temperature T from

$$\langle\mathcal{O}\rangle = g_s\mathrm{tr}\{\rho(\beta)\mathcal{O}\}/Z_N, \quad (2.14)$$

$$Z_N = g_s\mathrm{tr}\{\rho(\beta)\}, \quad (2.15)$$

where $\beta = 1/k_BT$ with k_B Boltzmann constant, $\mathrm{tr}\{\ldots\}$ is the trace over the spatial variables, Z_N the canonical partition function, $g_s = 2s+1$ is the spin degeneracy, and we assumed the Hamiltonian independent from spin. For *identical* bodies the spin-statistics theorem of quantum field theory, dictates that in spatial dimension bigger than two, particles with integer spin are bosons (obeying Bose-Einstein statistics, symmetric wave functions), while half-integer spin particles are fermions (obeying Fermi-Dirac statistics, antisymmetric wave functions). In dimension two anyonic statistics are also possible for identical and *impenetrable* bodies [59]. In this work, for bosons we will just consider the *spinless* $s = 0$ case, for fermions the spin $s = 1/2$ *fully polarized* case, with only one spin species, either all bodies spin up or all bodies spin down, and for anyons we make no assumption on their spin. In any case the measure (2.14) of the various thermodynamic or structural observables will not depend on g_s.

The position representation of the density matrix at an imaginary time $t = \beta$ is obtained through a *path integral*

$$\rho(R,R';\beta) = \langle R|\rho(\beta)|R'\rangle = \int \rho(R_0,R_1;\tau)\prod_{k=1}^{M-1}\left[\rho(R_k,R_{k+1};\tau)\sqrt{\tilde{g}(R_k)}\,dR_k\right] \times \delta(R_0-R)\delta(R_M-R')\,dR_0dR_M, \quad (2.16)$$

where we have discretized the imaginary time β into M*timeslices* with a small *timestep* $\tau = \beta/M$. The volume element of integration, $\sqrt{\tilde{g}(R)}\,dR$, can be treated by introducing $W(R) = -\ln[\sqrt{\tilde{g}(R)}]/\tau$ as an effective *geometrical potential*. The many-body path $R(t)$ is consequently discretized in M *beads* $R_k = (\{\boldsymbol{r}_{i,k}\}) = (\{r^\alpha_{i,k}\})$ at each timeslice $k = 1, 2, \ldots, M-1$. We will also call *link* a pair of contiguous beads. Note that to measure an observable through Eq. (2.14) it is necessary to consider closed paths such that $R(t+\beta) = R(t)$, or rings on the manifold $\mathcal{M}$.

For identical bodies, if they satisfy to the Bose-Einstein statistics, then one needs to symmetrize the distinguishable density matrix, and if they satisfy to the Fermi-Dirac statistics, then one needs to antisymmetrize it [60]. In these cases we can then write[10]

$$\rho_\pm(R,R';\beta) = \frac{1}{N!}\sum_{\mathcal{P}}\mathrm{sgn}(\mathcal{P})\rho(\mathcal{P}R,R';\beta), \quad (2.17)$$

$$\mathrm{sgn}(\mathcal{P}) = (\pm 1)^{\sum_{\nu=1}^N(\nu-1)C_\nu}, \quad (2.18)$$

where $\mathcal{P}$ is any permutation of the N particles such that $\mathcal{P}R = (\boldsymbol{r}_{\mathcal{P}1},\boldsymbol{r}_{\mathcal{P}2},\ldots,\boldsymbol{r}_{\mathcal{P}N})$, with sign $\mathrm{sgn}(\mathcal{P})$. Any permutations can be broken into cycles $\mathcal{P} = \{C_\nu\}$ where C_ν is

[5]The factor depending on the curvature of the manifold is due to Bryce DeWitt [54]. For a space of constant curvature there is clearly no effect, as the term due to the curvature just leads to a constant multiplicative factor that has no influence on the measure of the various observables.

[6]Remember that the metric tensor is covariantly constant.

[7]The expression for $\mathcal{K}$ is the one of Eq. (24.16) of Ref. [56] to lowest order in $R - R'$.

[8]See Ref. [23] for a numerical analysis of the accuracy of this approximation and for its possible refinements.

[9]For next orders corrections see, for example, Ref. [51].

[10]One can symmetrize or antisymmetrize respect to the first, the second or both the arguments of the distinguishable density matrix. We here choose the first case.

the number of cycles of length ν in $\mathcal{P}$. In the sum over the permutations one should use a $+1$ for the symmetrization necessary for bosons and -1 for the antisymmetrization necessary for fermions, in $\mathrm{sgn}(\mathcal{P})$. For example, for fermions, an even (odd) permutation has $\mathrm{sgn}(\mathcal{P}) = +1(-1)$ and an even (odd) number of exchanges of a pair of particles.

On a surface, $d = 2$, for impenetrable identical bodies, one can also have anyonic statistics [59]. In this case it is necessary to consider, more generally,

$$\rho_\nu(R, R'; \beta) = \sum_{\alpha\in B_N} \mathrm{Re}[\chi(\alpha)]\tilde{\rho}_\alpha(R, R'; \beta), \tag{2.19}$$

$$\chi(\{\text{paths } R(t) \text{ with } n \text{ braids among the pairs of single particle paths } \boldsymbol{r}(t)\}) = e^{-i\nu n\pi}, \tag{2.20}$$

where B_N is the infinite braid group which admits an infinite number of unitary one-dimensional representations χ, a phase factor, parametrized by an arbitrary number ν which determines the statistics and $\tilde{\rho}_\alpha$ is the distinguishable density matrix obtained from paths of kind α only. Clearly for $\nu = 0$ (mod 2) we recover the Bose-Einstein statistics and for $\nu = 1$ (mod 2) the Fermi-Dirac statistics. So we will be interested in values of $0 < \nu < 1$.

The braid group is the *fundamental group* of the quotient space $(S^{2N} - \Delta)/S_N$ where S^2 is the (two) sphere, $\Delta = \{R \mid \boldsymbol{r}_i = \boldsymbol{r}_j \text{ for some } i \neq j\}$, and S_N is the group of permutation of N bodies. We then see how paths $R(t)$ with different numbers of crossings between single-particle paths $\boldsymbol{r}(t)$ belong to different homotopy classes and one cannot be deformed continuously into the other. Therefore to take care of the density matrix of identical impenetrable bodies it is necessary to sum over all the topologically disjoint homotopy classes as is done in Eq. (2.19). If ν is rational, i.e., for *fractional statistics*, the phase factor will be periodic in n and for irrational ν, it will not.

For a two-dimensional electron gas in a transverse magnetic field the role of the Landau level [61] *filling factor* is played by the statistics ν [27,28] and certain fractional values for ν serve to explain the *fractional quantum Hall effect*. In particular, Laughlin [62] proposed an ansatz for the variational ground state of the *jellium* in a transverse magnetic field when the filling factor is $\nu = 1/p$ with p an odd integer. In his construction of the ground state trial wave function the exact analytic solution for the partition function of the one component (non quantum) plasma at a special value of the coupling constant [32,53] played a fundamental role. In this work we will not worry about introducing a magnetic field but we will study the case of the *electron gas* where the electrons, fermions, interact with a Coulomb pair potential on the manifold (see Sec. V).

We will now choose a particularly simple Riemannian manifold: the sphere!

III. THE SPHERE

A *sphere* of radius a is *the* (see 1839 Minding theorem and 1899 Liebmann theorem [63]) surface, $d = 2$,[11] of constant positive scalar curvature $2/a^2$ so that $\mathcal{R} = 2N/a^2$. Her metric is $ds^2 = g_{\alpha\beta}dr^\alpha dr^\beta = a^2(d\theta^2 + \cos^2\theta\, d\varphi^2)$.[12] The polar angle $r^1 = \theta \in]-\pi/2, \pi/2]$ and the azimuthal angle $r^2 = \varphi \in]-\pi, \pi]$ are the contravariant coordinates of the position vector $\boldsymbol{r} \in \mathcal{C}$, a point of the sphere, with $\mathcal{C} =]-\pi/2, \pi/2]\times]-\pi, \pi]$ the single-particle positions space. So that $\theta = 0$ is the *equator* and $\theta = \pm\pi/2$ are the *poles*. On the sphere $\sqrt{g(\boldsymbol{r})} = a^2|\cos\theta|$. And both the curvature term and the van Vleck factor, being constant, simply drop off from the measure of the various observables of Eq. (2.14).

The position of a particle on the sphere in the three-dimensional Euclidean space embedding the sphere is

$$\begin{aligned} x &= a\cos\theta\cos\varphi,\\ y &= a\cos\theta\sin\varphi,\\ z &= a\sin\theta, \end{aligned} \tag{3.1}$$

and the particle path on it is $\boldsymbol{q}(t) = (x(t), y(t), z(t))$.

The geodesic distance between particles $\boldsymbol{r}_i$ and $\boldsymbol{r}_j$ is

$$\begin{aligned} s_{ij} = s(\boldsymbol{r}_i, \boldsymbol{r}_j) = a \arccos\big[&\sin\left(r_i^1\right)\sin\left(r_j^1\right)\\ &+ \cos\left(r_i^1\right)\cos\left(r_j^1\right)\cos\left(r_i^2 - r_j^2\right)\big], \end{aligned} \tag{3.2}$$

whereas the Euclidean distance is

$$\begin{aligned} d_{ij} = d(\boldsymbol{r}_i, \boldsymbol{r}_j) &= a\sqrt{2(1 - \hat{\boldsymbol{q}}_i\cdot\hat{\boldsymbol{q}}_j)}\\ &= 2a\sin[\arccos(\hat{\boldsymbol{q}}_i\cdot\hat{\boldsymbol{q}}_j)/2], \end{aligned} \tag{3.3}$$

where $\hat{\boldsymbol{q}}_i = \boldsymbol{q}_i/a$ is the versor that from the center of the sphere points toward the center of the ith particle.

We use the Metropolis algorithm [64,65] to evaluate the average of Eq. (2.14). A code listing is offered in the Supplemental Material [66] (see also Ref. [1] therein).

To explore ergodically the positions space $\boldsymbol{r} = (\theta, \varphi) \in \mathcal{C}$ to sample the distinguishable density matrix we use the transition *displacement* move described in Appendix A.

To sample the permutation sum of Eq. (2.17) needed for identical bodies we use a transition move combination of two Brownian *bridges* between unlike bodies as described in Appendix B. To construct a single Brownian bridge it is essential to map, project, the sphere on a flat coordinate system. Our choice is presented in Appendix B. Perform the Gaussian bridge move in the projection flat space and then

[11] So it is conformally flat as any Riemannian manifold of dimension $d \leqslant 3$.

[12] Note that in the kinetic action of the path integral Monte Carlo calculation it is crucial to use consistently either $ds^2(\boldsymbol{r}, \boldsymbol{r}') = g_{\alpha\beta}(\boldsymbol{r})(\boldsymbol{r} - \boldsymbol{r}')^\alpha(\boldsymbol{r} - \boldsymbol{r}')^\beta$ or $ds^2(\boldsymbol{r}, \boldsymbol{r}') = g_{\alpha\beta}(\boldsymbol{r}')(\boldsymbol{r} - \boldsymbol{r}')^\alpha(\boldsymbol{r} - \boldsymbol{r}')^\beta$.

map it back to the sphere. The Metropolis algorithm will then allow to sample the high temperature density matrix whose kinetic action is not purely Gaussian on the sphere, due to the metric tensor appearing in $d\tilde{s}^2$.[13]

To sample the sum over the homotopy classes of Eq. (2.19) needed for identical (impenetrable) bodies we use a combination of bridge and displacement transition moves as described in Appendix C. Note that the displacement moves can be freely substituted by moves of bridges connecting only like bodies. But we found it convenient to use both moves for three reasons: (i) a Monte Carlo method usually becomes more efficient if implemented through a rich menu of different moves; (ii) from a purely formal point of view, one starts from simple single bead moves and only later builds more complex many beads moves; (iii) since the single bead displacement move is simple to construct it can serve as a test for more elaborated many beads moves.

We will work in the canonical ensemble with fixed number of particles N, surface area $A = 4\pi a^2$, surface density $\sigma = N/4\pi a^2$, and absolute temperature $T = 1/k_B\beta$. In our simulations we will only consider the $m = 1$ case. The many-body system *degeneracy parameter* is $\Theta = T/T_D$ where the degeneracy temperature $T_D = \sigma\hbar^2/mk_B$.[14] For temperatures higher than T_D, $\Theta \gg 1$, quantum effects are not very important and the distinction between distinguishable particles, bosons, fermions, or anyons is lost. We will treat both the noninteracting fluid $V = 0$ and the Coulomb fluid

$$V(R) = \sum_{i<j} \frac{e^2}{d_{ij}}, \tag{3.4}$$

where e is the unit of charge and we are assuming that the particles, moving on the sphere, interact with the three-dimensional pair Coulomb potential in terms of the Euclidean distance (3.3) between two electrons.[15] The *Coulomb coupling constant* is $\Gamma = \beta e^2/a_0 r_s$ with $a_0 = \hbar^2/me^2$ the Bohr radius and $r_s = (4\pi\sigma)^{-1/2}/a_0$ the Wigner-Seitz radius. At weak coupling, $\Gamma \ll 1$, the plasma becomes weakly correlated. Choosing length in units of the Wigner-Seitz radius, $a_0 r_s = a/\sqrt{N}$, and energy in units of Rydberg, $\mathrm{Ry} = \hbar^2/2ma_0^2$, we have $\lambda = 1/r_s^2$, $\Gamma = \beta(2/r_s)$, and $\Theta = (2\pi r_s^2)/\beta$. We then see that the kinetic energy scales as $1/r_s^2$ and the potential energy as $1/r_s$ so that the electron gas will approach the ideal gas limit at low r_s or high surface densities σ. In this work we will instead choose everywhere natural units, with $\hbar = k_B = 1$.

Apart from thermodynamic properties like the *kinetic energy* per particle e_K and the *potential energy* per particle e_V[16] we will also measure structural properties like the *radial distribution function*, $g(r) = \langle \mathcal{O} \rangle$. For it we may use the following histogram estimator:

$$O(R; r) = \sum_{i \neq j} \frac{1_{]r-\Delta/2, r+\Delta/2]}(d_{ij})}{N n_{id}(r)}, \tag{3.5}$$

where Δ is the histogram bin, $1_{]a,b]}(x) = 1$ if $x \in]a, b]$ and 0 otherwise, and

$$n_{id}(r) = N\left[\left(\frac{r + \Delta/2}{2a}\right)^2 - \left(\frac{r - \Delta/2}{2a}\right)^2\right] \tag{3.6}$$

is the average number of particles on the spherical crown $]r - \Delta/2, r + \Delta/2]$ for the ideal gas of density σ. We have that $\sigma^2 g(r)$ gives the probability, that sitting on a particle at $\boldsymbol{r}$, one finds another particle at $\boldsymbol{r}'$ with $r = d(\boldsymbol{r}, \boldsymbol{r}') \in [0, 2a]$. Note that $\sqrt{2a^2}$ is the Euclidean distance between a pole and a point on the equator. Alternatively one could consider a radial distribution function defined through the geodesic distance $r = s(\boldsymbol{r}, \boldsymbol{r}') \in [0, \pi a]$ where one chooses $1_{]r-\Delta/2, r+\Delta/2]}(s_{ij})$ in Eq. (3.5) with an appropriate normalization.[17]

For e_K and e_V we will use the *direct* estimator described in Ref. [23] applied to our action of Eq. (2.11). So that the kinetic energy per particle $e_K = \langle K(R_k, R_{k+1}; \tau)\rangle/N$ with $K(R, R'; \tau) = N/\tau - \tilde{g}_{\mu\nu}(R)(R - R')^\mu(R - R')^\nu/4\lambda\tau^2$ and the physical potential energy per particle $e_V = \langle V(R_k)\rangle/N$. During the simulation we will also measure the effective geometrical potential energy per particle $e_W = \langle W(R_k)\rangle/N$. For bosons we will also measure the *superfluid fraction* from the *area estimator* of Eqs. (4.1) and (4.2).

In Table I we list some case studies treated in our computer experiments. In all cases we use $M = 50$ timeslices and a surface density $\sigma = 1/10\pi$.

IV. NONINTERACTING BODIES

Here we will study noninteracting bodies with $\Gamma = 0$ or more generally $V = 0$. We are not aware of any analytic exact solution even for this simple case on the sphere. Whereas the flat case can be studied in closed form, but only in the grand canonical ensemble [68,69]. The noninteracting quantum many-body system on the sphere is equivalent to a noninteracting quantum many-body system on a plane under the influence of an effective external potential due to the curvature of the sphere [51].

A. Distinguishable bodies

Here we use the Metropolis algorithm with the transition displacement moves of Eqs. (A1) and (A2) or equivalently bridge moves of Eqs. (B1) and (B2) but between like particles.

---

[13] We tried to avoid passing back and forth through the projection mapping but with no results. In fact, to be able to construct a Brownian bridge it is necessary to connect particles several timeslices apart. And their geodesic distance s_{ij} does not reduce to a simple quadratic form.

[14] This is the temperature at which the size of a single-particle path, in absence of interaction, i.e., the thermal wavelength $(2\lambda\beta)^{1/2}$, equals the separation between single-particle paths, i.e., roughly $\sigma^{-1/2}$. Below this temperature it is possible for single-particle paths to link up exchanging their end points.

[15] Note that this is not the only possible choice since we could as well choose particles "living in" [67] the surface of the sphere as done for example in Refs. [41,43,44] (for other surfaces) or particle "moving on" the sphere but interacting with the two-dimensional logarithmic Coulomb potential with the Euclidean distance as done for example in Refs. [36,53].

[16] The estimators for these observables are carefully described in Ref. [23].

[17] In Ref. [19] we used the Euclidean distance.

TABLE I. Cases treated in our simulations: a the sphere radius, N the number of particles, β the inverse temperature, $e_K = \langle K\rangle/N$ the kinetic energy per particle from the thermodynamic estimator as explained in Ref. [23], $e_V = \langle V\rangle/N$ the physical potential energy per particle, and $e_W = \langle W\rangle/N$ the geometrical potential energy per particle. The other quantities were introduced in the main text. In the statistics column "d" stands for distinguishable, "b" for bosons, "f" for fermions, and "a" for anyons. The statistics $\nu \in [0, 1]$ is also reported. We chose natural units with $\hbar = k_B = 1$. The simulation lasted more than 10^8 Monte Carlo steps where one step is made of a displace move of all the beads of a single-particle path as described in Appendix A and a bridge move as described in Appendix B. Case F was the most computationally expensive and took roughly four weeks of computer time.

Case	Statistics	M	N	a	$a_0 r_s$	β	Γ	Θ	Ne_K	Ne_V	$-Ne_W$
A	d	50	10	5	$\sqrt{5/2}$	10	0	π	1.094(3)	0	148.39(5)
B	b $\nu = 0$	50	10	5	$\sqrt{5/2}$	100/3	0	$3\pi/10$	0.222(2)	0	44.46(1)
C	f $\nu = 1$	50	10	5	$\sqrt{5/2}$	100/3	0	$3\pi/10$	0.901(4)	0	44.47(1)
D	a $\nu = 1/2$	50	10	5	$\sqrt{5/2}$	100/3	0	$3\pi/10$	0.848(5)	0	44.43(1)
E	a $\nu = 1/3$	50	10	5	$\sqrt{5/2}$	100/3	0	$3\pi/10$	0.945(5)	0	44.64(1)
F	f $\nu = 1$	50	15	$5\sqrt{3/2}$	$\sqrt{5/2}$	100/3	$20\sqrt{10}\,e^2/3$	$3\pi/10$	1.655(4)	13.984(1)	75.232(8)
G	f $\nu = 1$	50	10	5	$\sqrt{5/2}$	100/3	$20\sqrt{10}\,e^2/3$	$3\pi/10$	1.133(4)	7.070(1)	44.202(8)
H	f $\nu = 1$	50	5	$5/\sqrt{2}$	$\sqrt{5/2}$	100/3	$20\sqrt{10}\,e^2/3$	$3\pi/10$	0.543(3)	2.0572(7)	16.952(8)
...											

In Fig. 1 we show a snapshot during the simulation for distinguishable noninteracting particles with $M = 50, N = 10, a = 5, \beta = 10$.

Many snapshots of the paths configurations during the simulation showed that the simulation "speed" of the beads of the paths near the poles gets small.[18] This is a consequence of the hairy ball theorem mentioned in the introduction. In fact, each link of the single-particle paths $\boldsymbol{r}(t)$ belongs to the tangent bundle of the sphere.

In Fig. 2 we show the radial distribution function, calculated by averaging the estimator of Eq. (3.5), for a gas of $N = 10$ distinguishable noninteracting particles on a sphere of radius $a = 5$ at an inverse temperature $\beta = 10$. We used $M = 50$ with only the displace move of Appendix A (this was used for Fig. 1) and with both the displacement move and the bridge move of Appendix B. From the figure we see how both the simulation with only the displacement move and the one with both the displacement and the bridge move give the expected result $g(r) = 1 - 1/N$, where the $1/N$ term takes care of the finite size of the system, for any M. This is a strong test on the correctness of our bridge move. We are then ready

[18] In fact, we have two different contributions responsible for this behavior: The g factor in the integration measure and the metric $g_{\mu\nu}$ in the kinetic action. These cannot be removed with a change of coordinates since it would require a *noncoordinate basis* [58].

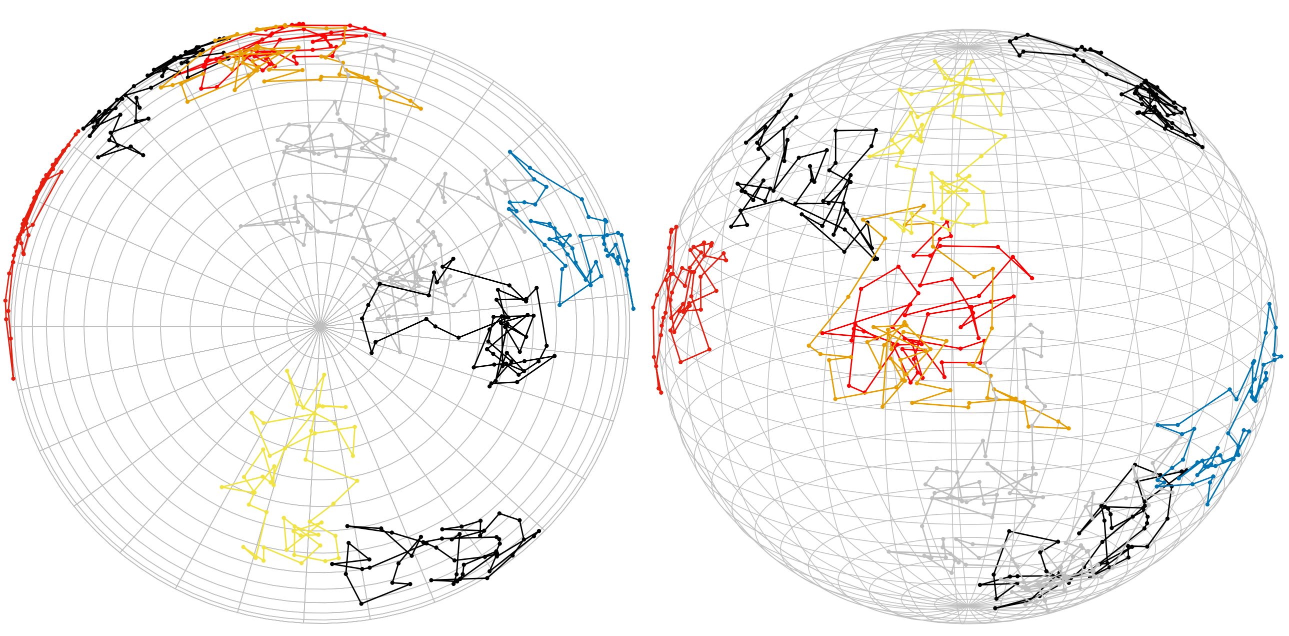

FIG. 1. Snapshot of the macroscopic path during the simulation for $N = 10$ noninteracting distinguishable particles with $M = 50$, $a = 5$, $\beta = 10$. Case A in Table I. The simulation started with all bodies distributed uniformly randomly on the equator. The different paths have different colors. In the left panel the top view and in the right panel the front view. In the simulation we measured $e_K = \langle \mathcal{K}\rangle = 1.089(4)$. Reducing β each path shrinks and tends to form a ring enclosing less amount of area.

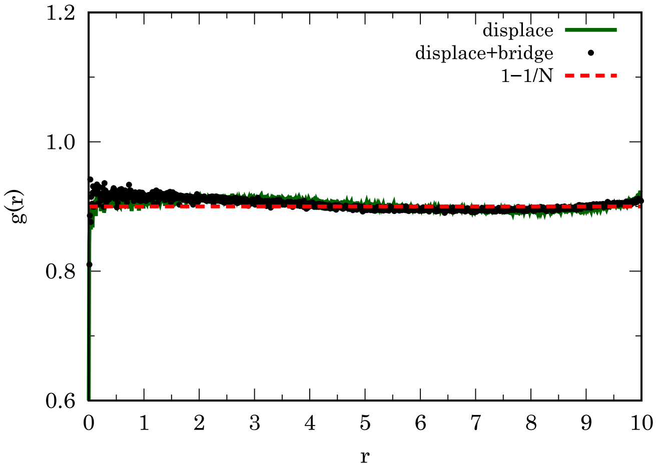

FIG. 2. Radial distribution function for the noninteracting distinguishable particles gas with $N = 10$ on a sphere of radius $a = 5$ at an inverse temperature $\beta = 10$. We use $M = 50$ (case A in Table I) with only the displace move of Appendix A and with both the displace and the bridge move as described in Appendix B. The dashed line is for $g(r) = 1 - 1/N = 0.9$.

to use it for the permutations sampling necessary for identical particles. We will do this in the next section.

B. Identical bodies

Here we use the Metropolis algorithm with the transition displacement moves of Eqs. (A1) and (A2) and bridge moves of Eqs. (B1) and (B2) between unlike particles as described in Appendix B to produce the necessary particles exchanges.

1. Bosons

Given the *superfluid* density σ_s and the *normal fluid* density $\sigma_n = 1 - \sigma_s$, the area estimator for the superfluid fraction is given by [23,70]

$$f_s = \frac{\sigma_s}{\sigma} = 1 - \frac{\sigma_n}{\sigma} = \frac{2m\langle \mathcal{A}^2\rangle}{\beta\lambda I_c}, \tag{4.1}$$

where, if ϵ is the Levi-Civita antisymmetric symbol, then

$$\mathcal{A} = \frac{1}{2}\sum_{i,k}\epsilon_{\alpha\beta}(r_{i,k+1} - r_k)^\alpha (r_{i,k+2} - r_{k+1})^\beta \sqrt{g(\boldsymbol{r}_{i,k+1})} \tag{4.2}$$

is the area enclosed by all the single-particle paths and I_c is the classical moment of inertia of the spherical shell that we will take as a fit parameter so that $\lim_{\beta\to\infty} f_s = 1$. Therefore our f_s is not an absolute superfluid fraction but a relative one. Moreover, we adapted to a curved surface the area estimator (4.1) that Ceperley and Pollock [see Sec. III E of Ref. [23] and Eq. (3.26) therein] derived for the Euclidean flat case. We did this by using for the area enclosed by all the single-particle paths the expression (4.2) valid for paths on the curved Riemannian surface. Our estimator (4.1) is an exact fluctuation-dissipation formula. Superfluidity is a microscopic property that can be defined in a finite system. It is not necessary to take the thermodynamic limit or to have a phase transition to see its effect. In the high temperature limit

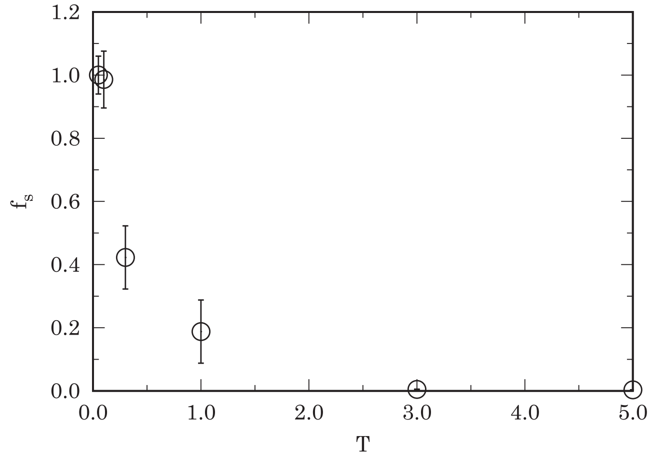

FIG. 3. Superfluid fraction (4.1) for the condensate of noninteracting bosons with $N = 10$, $a = 5$, $M = 50$. In this case $\tau \leqslant 0.4$ and $T_c = T_D \approx 0.0318$. The universal jump in f_s which would be expected at the superfluid phase transition is $(4m^2T_c/\sigma)/2\pi \approx 0.636$.

$f_s \to 0$ since the paths become short and straight and in the low temperature limit $f_s \to 1$ since the paths are long and the thermal average in σ_n sums up to zero.

In Ref. [71] Nelson and Kosterlitz use renormalization method of Ref. [72] to study the behavior of the superfluid density defined in Ref. [73] at the superfluid phase transition. They found that the superfluid density σ_s undergoes a *universal* jump equal to

$$\Delta\sigma_s = \frac{m^2}{\beta}\frac{2}{\pi}, \tag{4.3}$$

at the critical temperature, T_c, for the superfluid phase transition. This was also observed experimentally [74] for ^{4}He films. In the present language this says that the average squared area has a jump of $(I_c/\sigma)/2\pi$ at the transition. Naturally the phase transition can only occur in the thermodynamic limit [7] which in our case would correspond to the case of a degenerate sphere of an infinite radius, i.e., flat.

In Fig. 3 we show the superfluid fraction of Eq. (4.1) for the condensate of noninteracting bosons with $N = 10$, $a = 5$, $M = 50$. From the figure we see how the transition from $f_s = 0$ at high temperature to $f_s = 1$ at low temperature occurs in a temperature interval $\Delta T \approx 3$ and $f_s \approx 1$ is reached at the critical condensation temperature $T \approx T_D = 0.0318$ as expected.

In Fig. 4 we show a snapshot during the simulation for bosons noninteracting particles with $M = 50$, $N = 10$, $a = 5$, $\beta = 100/3$. We see how the system forms five permutation cycles corresponding to different colors.

In Fig. 5 we show the radial distribution function, calculated by averaging the estimator of Eq. (3.5), for the bosons noninteracting gas with $N = 10$ on a sphere of radius $a = 5$ at an inverse temperature $\beta = 100/3$ with $M = 50$. This is the same configuration used for Fig. 1 but at a lower temperature. The bump at $r = 0$ is a consequence of condensation predicted by the Bose-Einstein statistics which requires a symmetric density matrix respect to permutation of any two particles. Bosons like themselves [16] but on a sphere if they like

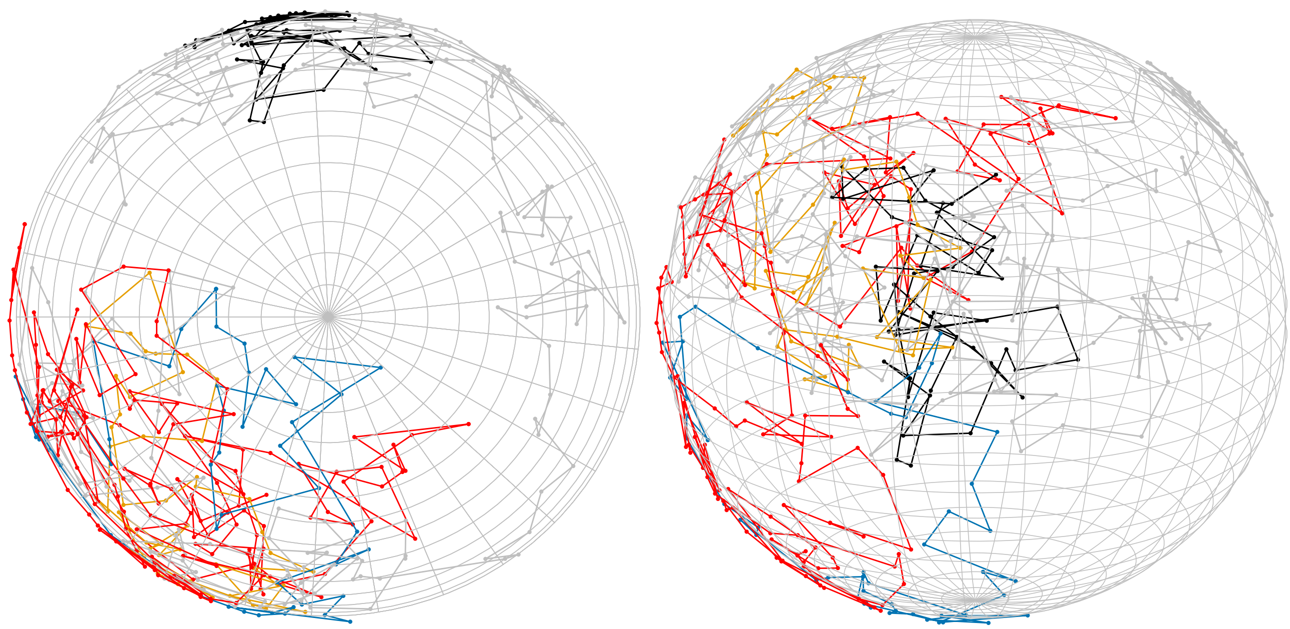

FIG. 4. Snapshot of the macroscopic path during the simulation for $N = 10$ noninteracting bosons with $M = 50$, $a = 5$, $\beta = 100/3$. Case B in Table I. The simulation started with all bodies distributed uniformly randomly on the equator. Paths corresponding to different permutations cycles have different colors. In the left panel the top view and in the right panel the front view. In the simulation we measured $e_K = \langle \mathcal{K} \rangle = 0.224(2)$. Reducing β each path shrinks and tends to form a ring enclosing less amount of area.

themselves near contact they must form a hole on the opposite point.

2. Fermions

Fermions properties cannot be calculated exactly with path integral Monte Carlo because of the *fermions sign problem* [22,60]. We then have to resort to an approximate calculation. The one we chose was the restricted path integral (RPIMC) approximation [16,19,22,60] with a "free fermions restriction." The trial density matrix used in the *restriction* is chosen as the one reducing to the ideal density matrix in the limit of $t \ll 1$ and is given by the following explicit analytic expression:

$$\rho_0(R', R; t) \propto \det||e^{-\frac{s^2(\mathbf{r}'_i, \mathbf{r}_j)}{4\lambda t}}||. \tag{4.4}$$

Note that here we need the geodesic distance between two particles on the sphere, $s^2(\mathbf{r}', \mathbf{r})$, that in the $t \ll 1$ limit reduces to $ds^2(\mathbf{r}', \mathbf{r}) = g_{\alpha\beta}(\mathbf{r})(\mathbf{r} - \mathbf{r}')^\alpha(\mathbf{r} - \mathbf{r}')^\beta$.

The *restricted path integral identity* that we will use states [22,60]

$$\rho_-(R', R; \beta) \propto \int \sqrt{\tilde{g}''} dR'' \, \rho_-(R'', R; 0) \tilde{\rho}_{\gamma_0(R'')}(R', R''; \beta), \tag{4.5}$$

where $\tilde{\rho}_{\gamma_0(R'')}(R', R''; \beta)$ is the distinguishable density matrix and the subscript means that we restrict the path integration in Eq. (2.16) to paths starting at R'', ending at R', and avoiding the nodes of ρ_0, i.e., to the *reach* of R'', $\gamma_0(R'')$. R'' will be called the *reference point* determining the reach. The nodes are on the reach boundary $\partial\gamma_0$. The weight of the walk is $\rho_-(R'', R; 0) = \det||\delta(\mathbf{r}''_i - \mathbf{r}_j)||$. Note that, in imposing the restriction it is convenient to imagine an infinitely positive external potential which will prevent a transition move $R \to R'$ such that $\rho_0(R', R; \tau) < 0$.[19] It is clear that the contribution of all the paths for a single element of the

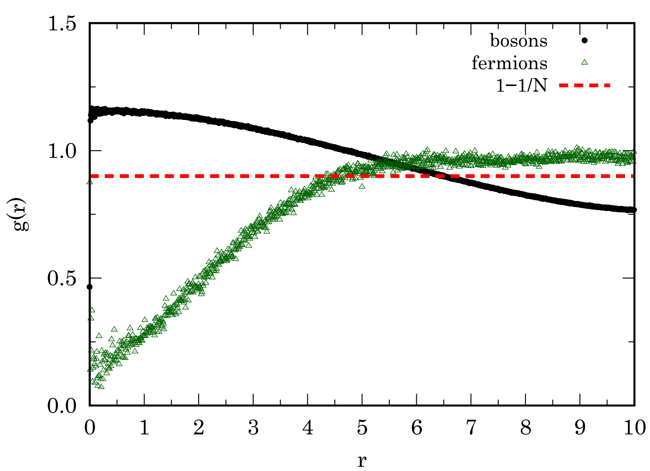

FIG. 5. Radial distribution function for the noninteracting bosons and fermions gas with $N = 10$ on a sphere of radius $a = 5$ at an inverse temperature $\beta = 100/3$ with $M = 50$. Case B and C in Table I, respectively. The dashed line is for $g(r) = 1 - 1/N = 0.9$. The bump at $r = 0$ for bosons is a manifestation of their tendency to like themselves. The exchange hole at $r = 0$ for fermions is a manifestation of their tendency to dislike themselves due to the Pauli exclusion principle and it requires $g(0) = 0$. The fact that $g(r)$ seems to approach not exactly 0 as $r \to 0$ is due to the path integral discretization error and we explicitly verified that choosing smaller timesteps τ, $g(0)$ comes even closer to 0.

[19] So that a move that changes the sign of ρ_0 are rejected in the Metropolis scheme.

density matrix will be of the same sign, thus solving the sign problem; positive if $\rho_-(R'', R; 0) > 0$, negative otherwise. On the diagonal any density matrix is positive and on the path restriction $\rho_-(R', R; \beta) > 0$, then only even permutations, those with $\mathrm{sgn}(\mathcal{P}) = +1$, are allowed, since $\rho_-(\mathcal{P}R, R; \beta) = \mathrm{sgn}(\mathcal{P})\rho_-(R, R; \beta)$. It is then possible to use a bosons calculation to get the fermions case. Clearly the restricted path integral identity with the free fermions restriction becomes exact if we simulate free fermions, but otherwise is just an approximation.

The restriction implementation is rather simple: we just reject the move whenever the proposed path is such that the ideal fermion density matrix (4.4) calculated between the reference point and any of the time slices subject to newly generated particles positions has a negative sign. So in correspondence of each displace move of Appendix A or bridge move of Appendix B it is necessary to calculate M determinants of order N. For this reason the method becomes unfeasible to treat systems with very many particles. To increase the acceptances in the restrictions, we found it convenient to choose the reference point time slice randomly, i.e., we choose an integer random number between 1 and M, say m, and the reference point is chosen to be $R = R_m$, before each move. This is allowed because we are free to perform a translation in the β-periodic imaginary thermal time.

In Fig. 5 we show the radial distribution function, calculated by averaging the estimator of Eq. (3.5), for the noninteracting, fully polarized fermions gas with $N = 10$ on a sphere of radius $a = 5$ at an inverse temperature $\beta = 100/3$ with $M = 50$. This is case C of Table I. The well at $r = 0$ is a consequence of Pauli exclusion principle predicted by the Fermi-Dirac statistics which requires an antisymmetric density matrix respect to permutation of any two particles. This well is usually called *exchange hole*. Fermions dislike themselves [16] but on a sphere if they dislike themselves at one point they must form a bump on the opposite point. A simple sum rule in this case requires $g(0) = 0$ since the the density matrix for coincident particles is singular and its determinant must be zero.

3. Anyons

Here we use the Metropolis algorithm with the transition displacement moves of Eqs. (A1) and (A2) and the swap moves of Eqs. (B1) and (B2) between two particles, as described in Appendix C, counting at each move the number of single-particle crossings n in the newly generated path R.

For example, from Eqs. (2.19) and (2.20) follows that, for $\nu = 1/2$,

$$\mathrm{Re}[\chi(\alpha)] = \begin{cases} (-1)^k & n = 2k, \\ 0 & n = 2k+1, \end{cases} \quad k = 0, 1, 2, 3, \dots . \tag{4.6}$$

We then see that to calculate $\rho_{1/2}$ necessary to simulate anyonic statistics for $\nu = 1/2$, one can simply use the RPIMC described above, to get rid of the sign problem, i.e., a bosonic PIMC with a restriction based on the nodes of the reference trial density matrix of Eq. (4.4), as for fermions. But now, after the Metropolis acceptance, we simply have to additionally throw away those moves that generate an odd number n of single-particle crossings, i.e., when $n = 1 \pmod 2$. To count the number n of braids we can proceed as described in Appendix C. Once again, as long as we have no interaction between the anyonic particles this scheme is expected to give rise to an exact computation.

However, we suspect that fractional statistics $\nu = q/p$ with $0 < q < p$ and $p > 2$ will give rise to fluids with different structure. For example, for $\nu = 1/3$ we find

$$\mathrm{Re}[\chi(\alpha)] = \begin{cases} (-1)^k & n = 3k, \\ (-1)^k \cos(\pi/3) & n = 3k+1, \quad k = 0, 1, 2, 3, \dots, \\ (-1)^k \cos(2\pi/3) & n = 3k+2, \end{cases} \tag{4.7}$$

and the $\rho_{2/3}$ should differ from the $\rho_{1/3}$. To simulate the $\nu = 1/3$ case we have to use again the RPIMC, to get rid of the sign problem, but now, differently from the $\nu = 1/2$ case, we have to weight each $\tilde{\rho}_\alpha$ with the correct factor, according to (4.7): 1 for $n = 3k$ and 1/2 otherwise. So that, after the Metropolis acceptance, if $n = 0 \pmod 3$ we do nothing and if $n \neq 0 \pmod 3$ we additionally throw away the moves with probability 1/2.

In Fig. 6 we show the radial distribution function, calculated by averaging the estimator of Eq. (3.5), for the noninteracting $\nu = 1/2$ and $\nu = 1/3$ anyons gas with $N = 10$ on a sphere of radius $a = 5$ at an inverse temperature $\beta = 100/3$ with $M = 50$. These are cases D and E of Table I. We compare them with the radial distribution for noninteracting fermions already shown in Fig. 5. From the comparison we can say that we observe a slight diminution of the exchange hole as we move from (fermions) $\nu = 1$ to (anyons) $\nu = 1/2$ to (anyons) $\nu = 1/3$. Moreover, we find $g_{1/3}(0) > g_{1/2}(0) > g_-(0) = 0$, where we indicate with g_ν the radial distribution function for statistics ν. The kinetic energy of the (anyons) $\nu = 1/2$ case is smaller than the one for $\nu = 1$ (fermions) and the one of the $\nu = 1/3$ case is bigger than the one for $\nu = 1$.

It would also be interesting to explore other rational cases $\nu = q/p$ with $0 < \nu < 1$ and see whether their structure differs in any way from the irrational cases.

V. ELECTRON GAS

In this section, we will study an electron gas, i.e., fermions interacting through the Coulomb potential of Eq. (3.4) with $e = 1$. We will only consider the fully polarized case where the density matrix is antisymmetric respect to permutation of any two particles. In this case we are unable to solve exactly the problem not even numerically with PIMC due to the fermions sign problem described above. We will then use the RPIMC with the ideal free fermions restriction based on the nodes of the reference density matrix of Eq. (4.4). This strategy, which is exact for noninteracting fermions, is here

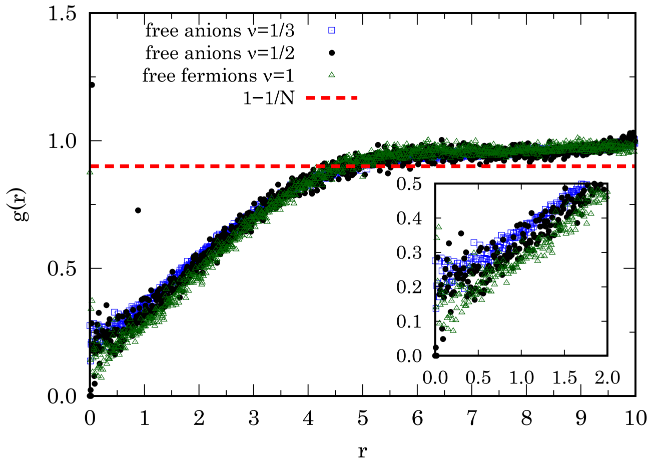

FIG. 6. Radial distribution function for the noninteracting $\nu = 1/2$ and $\nu = 1/3$ anyons gas with $N = 10$ on a sphere of radius $a = 5$ at an inverse temperature $\beta = 100/3$ with $M = 50$. Case D and E in Table I, respectively. The dashed line is for $g(r) = 1 - 1/N = 0.9$. From the inset we see how the structure of the free $\nu = 1/2$ anyons develops a slightly smaller exchange hole than fermions and the exchange hole of the free $\nu = 1/3$ anyons is slightly smaller than the one of the free $\nu = 1/2$ anyons.

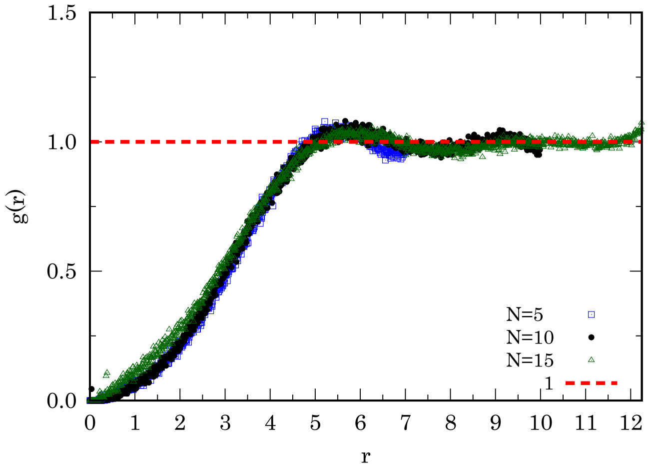

FIG. 7. Radial distribution function for the fully polarized electron gas interacting through the Coulomb potential of Eq. (3.4) with $e = 1$. We show cases F, G, and H of Table I at constant $\sigma = 1/10\pi$ and $N = 5,\ 10,\ 15$ electrons, respectively, at an inverse temperature $\beta = 100/3$ with $M = 50$. As the curvature increases at constant density, near contact the exchange-correlation hole tends to increase its extend and the long range oscillations around $g(r) = 1$ tend to to curl either upward or downward in a neighborhood of the ending point at $r = 2a$.

expected to become a better approximation at high density and high temperature, i.e., when correlation effects are weak.[20]

We simulated cases F, G, H of Table I where we keep constant the thermodynamic properties of the electron gas of temperature, $T = 3/100$, and surface density, $\sigma = 1/10\pi$, and increase gradually the radius of the sphere $a = 5/\sqrt{2}, 5, 5\sqrt{3/2}$. From a comparison of the results for the thermodynamic properties of the many-body system we see that the kinetic energy per particle remains approximately constant whereas the potential energy per particle diminishes as the curvature increases.

In Fig. 7 we show the radial distribution function for the electron gas of cases F, G, and H in Table I where we keep the surface density constant changing the number of particles $N = 5,\ 10,\ 15$, respectively. From the figure we see how the gas develops a *correlation hole* at $r = 0$ in addition to the exchange hole already shown in Fig. 5. The radial distribution function raises from $g(0) = 0$ at contact developing oscillations beyond a certain distance $r \gtrsim r_N$ around $g = 1$. From the comparison between cases F, G, and H we see how the *exchange-correlation hole* tends to increase as the curvature increases at constant surface density and at the same time $r_5 \approx r_{10} \approx r_{15} \approx 4.5$ and the oscillations tend to curl either upward or downward in a neighborhood of $r = 2a$.

VI. CONCLUSIONS

In this work we studied the effect of a constant positive curvature on a two-dimensional quantum many-body fluid. This is the simplest case that can be thought of in an exploration of the influence of curvature on the surface where the bodies move. At sufficiently low temperature quantum effects become important and the fluid will behave differently depending on the statistics ruling the bodies. The statistics depends on the transformation property of the many-body wave function under exchange of two bodies. If the bodies are distinguishable, then the wave function and its transformed will be different; if they are identical, then the transformed wave function can only be plus or minus the original wave function. The plus will be for bodies obeying to Bose-Einstein statistics and the minus for bodies obeying to the Fermi-Dirac statistics. If the identical bodies are also impenetrable, then the transformed wave function can more generally be the original wave function times a phase factor $e^{i\nu\pi}$, since, on a surface, exchanging the two particles by a clockwise rotation of π around their center of mass is a topologically and physically distinct operation than rotating counterclockwise. In this case the bodies are said to obey to the anyonic statistics, where the statistics is determined by the phase ν. For $\nu = 0$ (mod 2) one recovers the bosonic statistics and for $\nu = 1$ (mod 2) the fermionic statistics. While for bosons and fermions just the permutation of the particles in their initial and final configuration in imaginary time matters, for anyons it is also necessary to specify how the different trajectories wind or

[20]Note that in our implementation of the RPIMC we just added the approximate free-particle restriction to the exact PIMC for bosons. Doing like so we are neglecting almost all even permutations since our PIMC samples the permutations through the combination of two bridge and a swap moves as described in Appendix B but the restriction rejects almost all exchanges of two particles that would change the sign of the free-particle density matrix (4.4). To fully sample the even permutations in the RPIMC it is then necessary to add to our moves menu a third move which realizes a cyclic permutations of three particles 123 → 312. This will have no effect in the noninteracting case but is expected to become relevant in the interacting case. Here we simply neglected this third move even in the interacting case.

braid around each other during their imaginary time evolution. In other words the imaginary time evolution of the particles matters and cannot be neglected. The representation of the permutation group must be replaced by the one of the braid group.

We made some computer experiments for each one of these cases using a PIMC algorithm different from the one previously used in Refs. [19,20]. For the sign problem hidden in the Fermi-Dirac and the anyonic statistics we then used the RPIMC method. We studied both the case of the noninteracting bodies and for the fermions case the electron gas with a three-dimensional pair Coulomb interaction depending on the Euclidean distance between two electrons. In each case we measured the kinetic energy, the potential energy, and the radial distribution function. The pair correlation function of noninteracting fermions displays, at contact, the exchange hole and the one of the electron gas displays the exchange-correlation hole. While fermions dislike themselves due to the Pauli exclusion principle, bosons like themselves and form a condensate. This is reflected in a bump in the pair correlation function at contact. For bosons we also measured the superfluid fraction using an area estimator devised by Pollock and Ceperley. Even if on a finite sphere we clearly cannot reach the thermodynamic limit, the universal jump predicted by Nelson and Kosterlitz at the superfluid phase transition still gives some indications of the behavior of the superfluid fraction at the critical temperature.

The effect of curvature is then made manifest by comparing with similar studies in a flat Euclidean space in 3 dimensions [15,16] (compare, for example, our Fig. 5 with Fig. 3 in Ref. [16]) or in two dimensions [75–77]. Here we compared the electron gas at the same thermodynamic conditions of temperature and surface density on spheres of different radii. From the results of our computer experiments for cases F, G, and H of Table I we see that changing the curvature at constant density affects both the extent of the exchange correlation hole at contact and the oscillations at large distance. As the curvature increases the exchange-correlation hole tends to increase and the oscillations tend to curl either upward or downward at the pole opposite to contact. The kinetic energy per particle remains approximately constant upon changing the curvature whereas the physical and geometrical potential energy per particle diminish as the curvature increases.

During our simulations we made various snapshots of the many-body path configuration and we noticed that the simulation "speed" of the beads of the single-particle paths in proximity of the poles diminishes. We explained this occurrence as a consequence of the metric tensor properties which affect both the kinetic action and the path integral measure. A consequence of the "hairy ball theorem" which cannot be removed with a change of coordinates.

For the case of anyons we only considered the fractional statistics $\nu = 1/2$ and $\nu = 1/3$ in the noninteracting case. We found that the structure of the ideal anyons present an exchange hole that gets smaller moving from fermions with $\nu = 1$ to anyons with $\nu = 1/2$ and from anyons with $\nu = 1/2$ to anyons with $\nu = 1/3$. The kinetic energy of the $\nu = 1/2$ is smaller than the one for $\nu = 1$ and the one of the $\nu = 1/3$ is bigger than the one for $\nu = 1$.

It would be interesting to understand whether in the transition from a rational to an irrational statistics, there is any macroscopic observable change in the structure of the anyons fluid or in his thermodynamic properties.

In future computer experiments we plan to measure the effect of curvature on the pressure of the fluid as was done analytically in the nonquantum case in Ref. [41].

DATA AVAILABILITY

There are no publicly available research data or software supporting this manuscript. Requests for further information or data should be sent to the authors.

APPENDIX A: TRANSITION DISPLACEMENT MOVE

To explore the θ and φ positions space $\mathcal{C} =]-\pi/2, \pi/2]\times]-\pi, \pi]$ on the sphere it is convenient to propose the following displacement transition move for each particle in a randomly chosen bead of the many-body path

$$\theta_{\text{new}} = \theta_{\text{old}} + \Delta_\theta(\eta - 1/2), \tag{A1}$$

$$\varphi_{\text{new}} = \varphi_{\text{old}} + \Delta_\varphi(\eta - 1/2), \tag{A2}$$

where $\eta \in [0, 1]$ is a uniform pseudorandom number and Δ_θ and Δ_φ are two positive quantities measuring the θ displacement and the φ displacement, respectively.

This transition move can bring $\boldsymbol{r}_{\text{new}}$ out of $\mathcal{C}$ so it is also necessary to bring it back into $\mathcal{C}$ enforcing periodic boundary conditions $\varphi = \varphi + 2\pi$ and $\theta = \theta + \pi$ with the following subsequent chain of transformations

$$\begin{aligned} \theta_{\text{new}} &\to \theta_{\text{new}} - \pi\,\text{NINT}(\theta_{\text{new}}/\pi), \\ \varphi_{\text{new}} &\to \varphi_{\text{new}} - 2\pi\,\text{NINT}(\varphi_{\text{new}}/2\pi), \end{aligned} \tag{A3}$$

where `NINT` is the nearest integer function. One can easily convince himself that this chain does not alter the uniformity of the probability distribution of $\boldsymbol{r}_{\text{new}}$ in $\mathcal{C}$.

Note that the metric enters the free-particle variance since it is not possible by a change of coordinates to remove it both from the kinetic-action and from the integration measure $\sqrt{g(\boldsymbol{r})}\,d\boldsymbol{r}$, if not only locally. To take care of the metric factor in the integration measure it is convenient to introduce an effective/external single-particle geometrical potential $-\ln\sqrt{g(\boldsymbol{r})}/\tau$.

In the simulation we choose Δ_θ and Δ_φ so to have acceptance ratios as close as possible to 1/2 in the acceptance/rejection rule for the random walk transition displacement moves of the Metropolis algorithm. The transition probability distribution function for the displacement move of the Metropolis algorithm will be uniform so it will drop out of the acceptance probability distribution function.

APPENDIX B: TRANSITION BRIDGE MOVE

To take into account the particles permutations it is necessary to construct two Brownian bridges between two different[21] randomly chosen particles in two randomly chosen many-body beads to generate an exchange between the two particles. With one bridge we connect particle 1 on bead R_i to particle 2 on bead R_j and with the other we connect particle 2 on bead R_i to particle 1 on bead R_j with $i < j$. This will produce an *exchange* of particles 1 and 2.

The Brownian bridge between particle 1 at $\boldsymbol{r}_{1,i}$ and particle 2 at $\boldsymbol{r}_{2,j}$ is built through the following multislice transition move [23],

$$\boldsymbol{x}_{\text{new},i} = \boldsymbol{x}_{1,i}, \tag{B1}$$

$$\boldsymbol{x}_{\text{new},k} = \boldsymbol{x}_{\text{new},k-1} + \frac{\boldsymbol{x}_{2,j} - \boldsymbol{x}_{\text{new},k-1}}{j-k+1} + \xi \; k = i+1, \dots, j, \tag{B2}$$

where $\boldsymbol{x} = (\mathcal{X}, \mathcal{Y})$ is a two-dimensional vector on a flat space and ξ is a random number with a Gaussian probability distribution[22] with zero mean and variance $\sigma^2(j-k)/(j-k+1)$, where $\sigma^2 = 2\lambda\tau$ is the diagonal free-particle variance. We will then first perform a direct mapping $\theta \to \mathcal{X}$ and $\varphi \to \mathcal{Y}$. Then the bridge move of Eqs. (B1) and (B2). And finally we go back to the sphere with the inverse mapping $\mathcal{X} \to \theta$ and $\mathcal{Y} \to \varphi$. We will then have a direct mapping of the many-body system $R \to X = (\boldsymbol{x}_1, \boldsymbol{x}_2, \dots, \boldsymbol{x}_N) = (\{\boldsymbol{x}_i\})$ and an inverse mapping $X \to R$ back on the sphere.

The Metropolis (rejection) method can sample any probability distribution provided that the transition rule satisfies detailed balance and ergodicity. The Metropolis algorithm is a particular way of ensuring that the transition rule satisfies detailed balance. It does this by splitting the transition probability into an "*a priori*" *sampling distribution* $T(s \to s')$ (which is a probability distribution that we can sample) and an *acceptance probability* $A(s \to s')$ where $0 \leqslant A \leqslant 1$:

$$P(s \to s') = T(s \to s')A(s \to s'). \tag{B3}$$

In the generalized Metropolis procedure [65], trial moves are accepted according to

$$A(s \to s') = \min[1, q(s \to s')], \tag{B4}$$

where

$$q(s \to s') = \frac{\pi(s')T(s' \to s)}{\pi(s)T(s \to s')}, \tag{B5}$$

where $\pi \propto e^{-\mathcal{S}}$ is the action probability distribution in the $s = (\{R_k\}, \mathcal{P})$ configurations space. The transition probability corresponding to the move of Eqs. (B1) and (B2) is then given by

$$\frac{T(s_{\text{new}} \to s_{\text{old}})}{T(s_{\text{old}} \to s_{\text{new}})} \propto \exp\left[\sum_{k=i+1}^{j} (X_{\text{new},k} - X_{\text{new},k-1})^2/4\lambda\tau - \sum_{k=i+1}^{j} (X_{\text{old},k} - X_{\text{old},k-1})^2/4\lambda\tau\right]. \tag{B6}$$

So we start from R_{old} map it to X_{old}, on the direct mapping flat space perform the Brownian bridge move, accept or reject the transition according to the probability (B4) to find X_{new}, and finally inverse map it back to R_{new} on the sphere. Ergodicity in $\mathcal{Y}$ would be lost only if we are *exactly* on a pole. But this is always prevented on a computer due to the finite arithmetic! Moreover, since we have ergodicity everywhere in $\mathcal{X}$ it will always be possible to escape a pole by moving along $\mathcal{X}$.

To produce an exchange of two particles 1 and 2 one needs a combination of two bridge transitions as described above. Any permutation can be reached through a two particles exchange so the bridge transition move allows to sample the sum in Eq. (2.17).

APPENDIX C: BRAIDS SAMPLING

To sample the sum in Eq. (2.19) one needs a move able to bring the path $R(t)$ from one homotopy class to another. And a way to understand to which homotopy class the path belongs after each move. This will allow one to determine to which $\tilde{\rho}_\alpha$ he is contributing at each accepted transition move.

A path $R(t)$ made of closed distinct single-particle paths, $\boldsymbol{r}(0) = \boldsymbol{r}(\beta)$, on a sphere, can only have an even number n of two particles crossings, i.e., of braids. Allowing for particles exchanges n can be any integer. If two different particles, say 1 and 2, have m crossings between timeslices k_i and k_f, an acceptance of the swap move described in Appendix B, will necessarily result in a single crossing if m is even, and consequently $n \to n - m + 1$, or to no crossing at all, if m is odd, and consequently $n \to n - m$.

We see then how we can use the swap move to jump from any homotopy class to any other. And within an homotopy class α we can then act with the displace move described in Appendix A to sample $\tilde{\rho}_\alpha$.

To count the number of crossings between particles 1 and 2 between timeslices k_i and k_f it is necessary to count the number of times in which $\boldsymbol{r}_{1,k} = \boldsymbol{r}_{2,k}$ for $k \in [k_i, k_f]$. To take into account of this crossing condition in the discretized imaginary time one can for example determine when both $r^\alpha_{1,k} - r^\alpha_{2,k}$ for $\alpha = 1, 2$ change sign or are zero, varying k. Counting the number n of braids reached in the path $R(t)$ allows to asses to which path homotopy class one is contributing in the density matrix. So at each move we need to count the number of crossings n in the whole many-body path R_k from $k_i = 0$ to $k_f = M$.

[21] A bridge between the same particle can still be used to sample the density matrix of distinguishable particles as can be done with the displacement move of Appendix A.

[22] This can be generated with the Box-Muller algorithm [65], for example.

[1] J. R. Klauder and R. Fantoni, The magnificent realm of affine quantization: Valid results for particles, fields, and gravity, Axioms **12**, 911 (2023).

[2] R. Fantoni, *Unifying Classical and Quantum Physics—How Classical and Quantum Physics Can Pass Smoothly Back and Forth* (Springer, New York, NY, 2025).

[3] A. Tononi and L. Salasnich, Low-dimensional quantum gases in curved geometries, Nat. Rev. Phys. **5**, 398 (2023).

[4] A. Tononi and L. Salasnich, Shell-shaped atomic gases, Phys. Rep. **1072**, 1 (2024).

[5] A. Tononi and L. Salasnich, Bose-Einstein condensation on the surface of a sphere, Phys. Rev. Lett. **123**, 160403 (2019).

[6] A. Tononi, F. Cinti, and L. Salasnich, Quantum bubbles in microgravity, Phys. Rev. Lett. **125**, 010402 (2020).

[7] A. Tononi, A. Pelster, and L. Salasnich, Topological superfluid transition in bubble-trapped condensates, Phys. Rev. Res. **4**, 013122 (2022).

[8] A. Tononi, Scattering theory and equation of state of a spherical two-dimensional Bose gas, Phys. Rev. A **105**, 023324 (2022).

[9] M. Ciardi, F. Cinti, G. Pellicane, and S. Prestipino, Supersolid phases of bosonic particles in a bubble trap, Phys. Rev. Lett. **132**, 026001 (2024).

[10] A. Tononi and G. E. Astrakharchik, Bose-Einstein condensation on axially-symmetric surfaces, Phys. Rev. A **112**, 023302 (2025).

[11] M. Ciardi, F. Cinti, G. Pellicane, and S. Prestipino, Effects of gravity on supersolid order in bubble-trapped bosons, Phys. Rev. B **111**, 024512 (2025).

[12] https://en.wikipedia.org/wiki/List_of_fusion_experiments.

[13] S. D. Kenny, G. Rajagopal, R. J. Needs, W.-K. Leung, M. J. Godfrey, A. J. Williamson, and W. M. C. Foulkes, Quantum Monte Carlo calculations of the energy of the relativistic homogeneous electron gas, Phys. Rev. Lett. **77**, 1099 (1996).

[14] E. W. Brown, B. K. Clark, J. L. DuBois, and D. M. Ceperley, Path-integral Monte Carlo simulation of the warm dense homogeneous electron gas, Phys. Rev. Lett. **110**, 146405 (2013).

[15] R. Fantoni, Jellium at finite temperature using the restricted worm algorithm, Eur. Phys. J. B **94**, 63 (2021).

[16] R. Fantoni, Jellium at finite temperature, Mol. Phys. **120**, e1996648 (2022).

[17] D. M. Ceperley and B. J. Alder, The calculation of the properties of metallic hydrogen using Monte Carlo, Phys. B **108**, 875 (1981).

[18] D. M. Ceperley and B. J. Alder, Ground state of solid hydrogen at high pressure, Phys. Rev. B **36**, 2092 (1987).

[19] R. Fantoni, One-component fermion plasma on a sphere at finite temperature, Int. J. Mod. Phys. C **29**, 1850064 (2018).

[20] R. Fantoni, One-component fermion plasma on a sphere at finite temperature. The anisotropy in the paths conformations, J. Stat. Mech. (2023) 083103.

[21] D. M. Ceperley and B. J. Alder, Ground state of the electron gas by a stochastic method, Phys. Rev. Lett. **45**, 566 (1980).

[22] D. M. Ceperley, Fermion nodes, J. Stat. Phys. **63**, 1237 (1991).

[23] D. M. Ceperley, Path integrals in the theory of condensed helium, Rev. Mod. Phys. **67**, 279 (1995).

[24] R. Fantoni, Statistical gravity through affine quantization, Quantum Rep. **6**, 706 (2024).

[25] R. Fantoni, Statistical gravity and entropy of spacetime, Stats **8**, 23 (2025).

[26] R. Fantoni, Statistical gravity, ADM splitting, and affine quantization, Gravitat. Cosmol. **31**, 568 (2025).

[27] G. O. V. Melik-Alaverdian and N. E. Bonesteel, Fixed-phase diffusion Monte Carlo study of the quantum-Hall effect on the Haldane sphere, Phys. E **1**, 138 (1997).

[28] G. Melik-Alaverdian, N. E. Bonesteel, and G. Ortiz, Quantum Hall fluids on the Haldane sphere: A diffusion Monte Carlo study, Phys. Rev. Lett. **79**, 5286 (1997).

[29] V. Melik-Alaverdian, G. Ortiz, and N. E. Bonesteel, Quantum projector method on curved manifolds, J. Stat. Phys. **104**, 449 (2001).

[30] J. Ginibre, Statistical ensembles of complex, quaternion, and real matrices, J. Math. Phys. **6**, 440 (1965).

[31] M. L. Metha, *Random Matrices* (Academic, New York, NY, 1967).

[32] B. Jancovici, Exact results for the two-dimensional one-component plasma, Phys. Rev. Lett. **46**, 386 (1981).

[33] A. Alastuey and B. Jancovici, On the classical two-dimensional one-component Coulomb plasma, J. Phys. France **42**, 1 (1981).

[34] P. Choquard, Helv. Phys. Acta **54**, 332 (1981).

[35] P. Choquard, P. J. Forrester, and E. R. Smith, The two-dimensional one-component plasma at $\Gamma = 2$: The semiperiodic strip, J. Stat. Phys. **33**, 13 (1983).

[36] J. M. Caillol, Exact results for a two-dimensional one-component plasma on a sphere, J. Phys. Lett. **42**, 245 (1981).

[37] G. Téllez and P. J. Forrester, Exact finite-size study of the 2D OCP at $\Gamma = 4$ and $\Gamma = 6$, J. Stat. Phys. **97**, 489 (1999).

[38] B. Jancovici, Pressure and Maxwell tensor in a Coulomb fluid, J. Stat. Phys. **99**, 1281 (2000).

[39] R. P. Salazar and G. Téllez, Exact energy computation of the one component plasma on a sphere for even values of the coupling parameter, J. Stat. Phys. **164**, 969 (2016).

[40] B. Jancovici and G. Téllez, Two-dimensional Coulomb systems on a surface of constant negative curvature, J. Stat. Phys. **91**, 953 (1998).

[41] R. Fantoni, B. Jancovici, and G. Téllez, Pressures for a one-component plasma on a pseudosphere, J. Stat. Phys. **112**, 27 (2003).

[42] B. Jancovici and G. Téllez, Charge fluctuations for a Coulomb fluid in a disk on a pseudosphere, J. Stat. Phys. **116**, 205 (2004).

[43] R. Fantoni and G. Téllez, Two dimensional one-component plasma on a Flamm's paraboloid, J. Stat. Phys. **133**, 449 (2008).

[44] R. Fantoni, Two component plasma in a Flamm's paraboloid, J. Stat. Mech. (2012) P04015.

[45] J. Tempere, I. F. Silvera, and J. T. Devreese, Many-body properties of a spherical two-dimensional electron gas, Phys. Rev. B **65**, 195418 (2002).

[46] E. Artin, Theory of braids, Ann. Math. **48**, 101 (1947).

[47] R. Fantoni, Johannes W. O. Salari, and B. Klumperman, The structure of colloidosomes with tunable particle density: Simulation vs experiment, Phys. Rev. E **85**, 061404 (2012).

[48] H. Poincaré, Sur les courbes dfinies par les équations différentielles, J. Math. Pures Appl. **1**, 167 (1885).

[49] L. E. J. Brouwer, Über abbildung von mannigfaltigkeiten, Math. Ann. **71**, 97 (1911).

[50] H. Hopf, Vektorfelder in n-dimensionalen mannigfaltigkeiten, Math. Ann. **96**, 209 (1927).

[51] F. Bastianelli and O. Corradini, On the simplified path integral on spheres, Eur. Phys. J. C **77**, 731 (2017).

[52] E. Artin, Ein mechanisches System mit quasi-ergodischen Bahnen, Abh. Math. Semin. Univ. Hambg. **3**, 170 (1924).

[53] R. Fantoni, Plasma living in a curved surface at some special temperature, Phys. A **524**, 177 (2019).

[54] B. S. DeWitt, Dynamical theory in curved spaces. I. A review of the classical and quantum action principles, Rev. Mod. Phys. **29**, 377 (1957).

[55] J. H. V. Vleck, The correspondence principle in the statistical interpretation of quantum mechanics, Proc. Natl. Acad. Sci. USA **14**, 178 (1928).

[56] L. S. Schulman, *Techniques and Applications of Path Integration* (John Wiley & Sons, Technion, Haifa, Israel, 1981), Chap. 24.

[57] H. F. Trotter, On the product of semi-groups of operators, Proc. Am. Math. Soc. **10**, 545 (1959).

[58] C. W. Misner, K. S. Thorne, and J. A. Wheeler, *Gravitation* (W. H. Freeman, San Francisco, CA, 1973).

[59] A. Lerda, *Anyons. Quantum Mechanics of Particles with Fractional Statistics* (Springer-Verlag, Berlin, 1992).

[60] D. M. Ceperley, Path integral Monte Carlo methods for fermions, in *Monte Carlo and Molecular Dynamics of Condensed Matter Systems*, edited by K. Binder and G. Ciccotti (Editrice Compositori, Bologna, Italy, 1996).

[61] L. D. Landau and E. M. Lifshitz, in *Quantum Mechanics*, edited by E. M. Lifshitz and L. P. Pitaevskii, Sec. 111, 112, Course of Theoretical Physics Vol. 3 (Butterworth Heinemann, Oxford, 1977).

[62] R. B. Laughlin, Anomalous quantum Hall effect: An incompressible quantum fluid with fractionally charged excitations, Phys. Rev. Lett. **50**, 1395 (1983).

[63] A. Gray, *Modern Differential Geometry of Curves and Surfaces with Mathematica*, 2nd ed. (CRC Press, Boca Raton, FL, 1997), pp. 652–654.

[64] N. Metropolis, A. W. Rosenbluth, M. N. Rosenbluth, A. M. Teller, and E. Teller, Equation of state calculations by fast computing machines, J. Chem. Phys. **21**, 1087 (1953).

[65] M. H. Kalos and P. A. Whitlock, *Monte Carlo Methods* (John Wiley & Sons, New York, NY, 1986).

[66] See Supplemental Material at http://link.aps.org/supplemental/10.1103/y457-glbg for a listing of the FORTRAN code used in the simulations.

[67] E. A. Abbott, *Flatland: A Romance of Many Dimensions* (Seeley & Co., London, UK, 1884).

[68] R. P. Feynman, in *Statistical Mechanics: A Set of Lectures*, edited by Jacob Shaham, Frontiers in Physics Vol. 36, (W. A. Benjamin, New York, NY, 1972).

[69] R. Fantoni, Thermodynamic limit of the free electron gas on a circle, Phys. Educ. **06**, 2450012 (2024).

[70] E. L. Pollock and D. M. Ceperley, Path-integral computation of superfluid densities, Phys. Rev. B **36**, 8343 (1987).

[71] D. R. Nelson and J. M. Kosterlitz, Universal jump in the superfluid density of two-dimensional superfluids, Phys. Rev. Lett. **39**, 1201 (1977).

[72] J. V. José, L. P. Kadanoff, S. Kirkpatrick, and D. R. Nelson, Renormalization, vortices, and symmetry-breaking perturbations in the two-dimensional planar model, Phys. Rev. B **16**, 1217 (1977).

[73] R. P. Feynmann, Application of quantum mechanics to liquid helium, Prog. Low Temp. Phys. **1**, 17 (1955).

[74] D. J. Bishop and J. D. Reppy, Study of the superfluid transition in two-dimensional ^{4}He films, Phys. Rev. Lett. **40**, 1727 (1978).

[75] B. Tanatar and D. M. Ceperley, Ground state of the two-dimensional electron gas, Phys. Rev. B **39**, 5005 (1989).

[76] W. R. Magro and D. M. Ceperley, Ground state properties of the two-dimensional Bose Coulomb liquid, Phys. Rev. Lett. **73**, 826 (1994).

[77] M. C. Gordillo and D. M. Ceperley, Path-integral calculation of the two-dimensional ^{4}He phase diagram, Phys. Rev. B **58**, 6447 (1998).